01 Apr 1993

Residual-Ion Orientation After Autoionization

G. T. Xu

Xiao Wang

J. Greg Story
Missouri University of Science and Technology, story@mst.edu

William E. Cooke

RAPID COMMUNICATIONS

PHYSICAL REVIEW A VOLUME 47, NUMBER 4 APRIL 1993

Residual-ion orientation after autoionization

G. T. Xu, Xiao Wang, J. G. Story,* and W. E. Cooke

Department of Physics, University of Southern California, Los Angeles, California 90089-0484

(Received 5 November 1992)

We have measured the relative population in the two m_j states of barium $6p_{1/2}$ ions produced by the autoionization of $(6p_{3/2}nd)_{J=M_J=3}$ states by detecting the helicity of the emitted fluorescence. These populations can be related to the relative branching ratio into the $6p_{1/2}\epsilon d_{5/2}$ and $6p_{1/2}\epsilon g_{7/2}$ continuum channels. Rydberg states with n=16–23 have similar branching ratios, producing approximately six times as much $6p_{1/2}\epsilon d_{5/2}$ population as $6p_{1/2}\epsilon g_{7/2}$ population.

PACS number(s): 32.80.Dz

The $(6pnd)_{J=M_J=3}$ autoionizing states of barium have been studied by Gounand *et al.* [1], and Mullins *et al.* [2] as an example of selecting a specific J state using circularly polarized lasers in the isolated core excitation (ICE) method [3]. Although there are a total of 60 possible $6pnd$ states, restricting J and M_J reduces the number of states to only three — one $6p_{1/2}nd$ state, which is well separated from two $6p_{3/2}nd$ states [which were designated $(6p_{3/2}nd)^+$ and $(6p_{3/2}nd)^-$ by Gounand *et al.* [1]]. The two $6p_{3/2}nd$ states have identical symmetry and are separated by less than their linewidths, and so they are not really separate eigenstates. Any excitation creates a coherent superposition of the + and − characters; however, the ICE spectra of these resonances are nearly symmetric, and each is reached via a different intermediate state, so that the + and − state designation is approximately valid and certainly convenient. The earlier measurements concentrated on the position, autoionization-broadened linewidth, and transition moments of these states, thereby determining the composition of the $(6p_{3/2}nd)^+$ and $(6p_{3/2}nd)^-$ characters, and the interactions between the different series. No attempt has yet been made to measure the branching ratios into different continuum channels directly, because the excitation requires three circularly polarized lasers, and this forces the symmetry axis to be the laser propagation direction. Thus, an angular distribution measurement would require a movable electron detector, whereas all the electron angular distribution studies to date have merely rotated the polarization axis of a linearly polarized laser [4, 5].

Here, we report a measurement of the relative branching ratio between the two $6p_{1/2}\epsilon l_j$ continuum channels by employing an extension of the residual-ion fluorescence detection technique [6]. With an improved detection system, we can now selectively monitor either *helicity* of the residual-ion fluorescence. This enables us to detect signals from each of the two m_j states of the $6p_{1/2}$ barium ion. When the $(6p_{3/2}nd)_{J=M_J=3}$ state autoionizes to the $6p_{1/2}$ continuum, the $\epsilon d_{5/2}$ channel may only produce $6p_{1/2}$ ions in the $m_j = +1/2$ state, to conserve J and M_J. The $\epsilon g_{7/2}$ channel may produce either ion state; however, a simple angular-momentum calculation shows that a $(6p_{1/2}\epsilon g_{7/2})_{J=M_J=3}$ wave produces seven times as many $m_j = -1/2$ ions as $m_j = +1/2$ ions. Consequently, the helicity-sensitive detection effectively separates the signals from the $\epsilon d_{5/2}$ and $\epsilon g_{7/2}$ channels.

We excited the $(6p_{3/2}nd)_{J=M_J=3}$ states using standard ICE techniques [3]; however, we simultaneously collected the total ion signal and the polarized fluorescence from the $6p_{1/2}$ ions. As shown in Fig. 1, two lasers excited the bound $6snd$ Rydberg states of barium, and a third laser then excited the core transition.

The first laser, at 553 nm, excited barium atoms in an effusive atomic beam from the ground state to the $6s6p\ ^1P_1$ state, and the second laser, near 420 nm, then excited the atom further to the $6snd\ ^1D_2$ state. After a delay of about 30 ns, the third (or core) laser, near 455 nm, excited the $6s_{1/2} \rightarrow 6p_{3/2}$ core transition, and populated the $(6p_{3/2}nd)_{J=M_J=3}$ autoionizing state. The delay before the core excitation allowed the $6s6p\ ^1P_1$ states to decay back to the ground state in order to prevent a large marker resonance from the strong, two step, $6s6p\ ^1P_1 \rightarrow 6s10d\ ^1D_2 \rightarrow 6p_{3/2}10d$ transition. All the lasers were circularly polarized in the same sense to reach the final $J=M_J=3$ state. Furthermore, by selecting the singlet $6snd\ ^1D_2$ intermediate state, the core excitation primarily excites the $(6pnd)^+_{J=M_J=3}$ character [2, 7].

The third harmonic of the same Nd:YAG (neodymium -doped yttrium aluminum garnet) laser pumps all three dye lasers. The pump laser has a 10-ns pulse width,

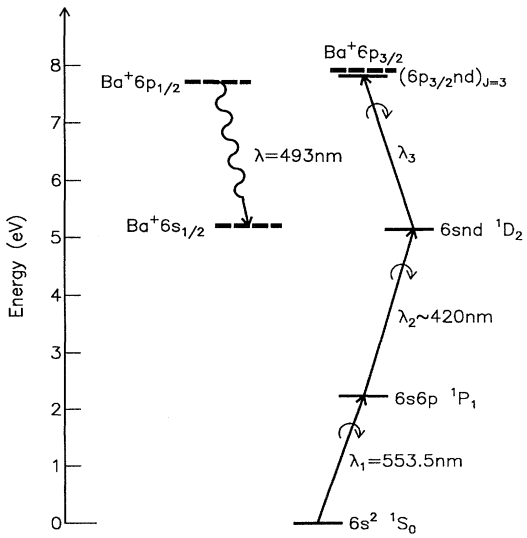

FIG. 1. The energy-level diagram of barium showing the excitation of the $(6p_{3/2}nd)_{J=M_J=3}$ states, and the detection of fluorescence from the resulting $6p_{1/2}$ ions.

and each resulting dye laser typically has a linewidth of 0.5 cm^{-1} and a pulse length of 5 ns. We combined the laser beams collinearly and polarized them with a linear polarizer before they passed through a Fresnel rhomb to generate the circular polarization. All three laser powers were attenuated such that none of the transitions was saturated.

A schematic diagram of the apparatus is shown in Fig. 2. The barium source is in a screw-top stainless-steel oven with a 1.5-mm nozzle drilled in the top. We typically heat the oven to a temperature of 800 °C to produce a density in the interaction region of $10^{10} - 10^{11}$ atoms/cm^3, while maintaining a base pressure of approximately 10^{-6} torr. The ion detector consists of a pair of parallel-plate conductors, separated by 5 cm, with one plate (called the front plate) having the central region replaced by a stainless-steel mesh screen. A dual-microchannel plate (MCP) is mounted 10 cm beyond the front plate, so that the ions produced by autoionization can be collected by pulsing the back plate with approximately +600 v, 1 μs after the third laser. The ion collection direction is perpendicular to both the atomic beam, and to the excitation lasers. Three sets of magnetic field coils balance the magnetic field of the earth and any other sources, and maintain a small field (typically 2.5 G) in the laser propagation direction to stabilize the quantization axis.

The fluorescence detection system consists of a spherical mirror with diameter of 5 cm and focal length of 6 cm followed by a flat front-surface mirror at 45°. The excitation lasers pass directly through a 5-mm hole in the center of each mirror and exit the chamber through a window. The spherical mirror sits before the interaction region with the focal point at the spot where the laser beams intersect the atomic beam. The flat mirror sits after the interaction region to redirect the fluorescence out of the laser beam path. Thus, we collected a near-axis backward fluorescence signal as a parallel beam and maintained its helicity. Our helicity detection system is a quarter-wave plate followed by a linear polarizer, a condensing lens, an interference filter, and a phototube. The flat mirror does introduce a slight phase shift; however, this can be minimized by adjusting the angle of the linear polarizer in the detection system. A laboratory microcomputer scans the frequency of the core laser and records the ion and polarized fluorescence signals after they are accumulated by boxcar integrators. By monitoring fluorescence and ion signals simultaneously and taking the ratio of the two, we greatly reduced the noise due to shot-to-shot fluctuation and long-term laser power drift. Figure 3 shows typical fluorescence data for the $(6p_{3/2}19d)_{J=3}$ state, where (a) shows the fluorescence signal from $6p_{1/2}$ ($m_j = +1/2$) ions, while (b) shows the fluorescence signal from the $6p_{1/2}$ ($m_j = -1/2$) ions.

In Fig. 4(a), we have constructed the relative branching ratios for the $m_j = +1/2$ ion state (o) and for the $m_j = -1/2$ ion state (+) by dividing each fluorescence signal by the corresponding ion signal obtained during that scan. These branching ratios have been normal-

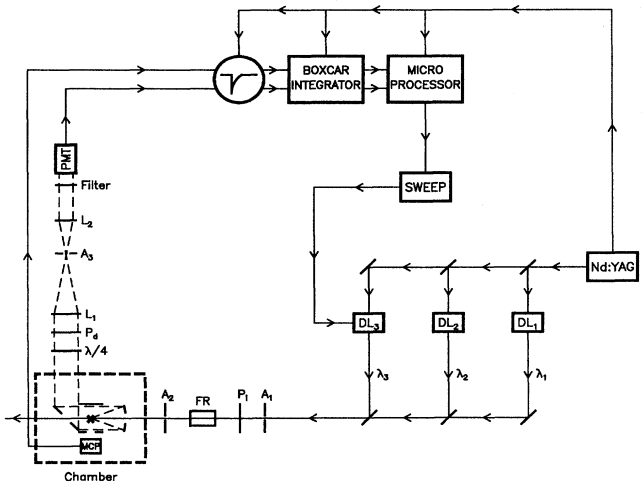

FIG. 2. A schematic diagram of the apparatus for the excitation of the $(6p_{3/2}nd)_{J=M_J=3}$ states of barium, and the detection of the total ion and the polarized fluorescence from the resulting $6p_{1/2}$ ions. The excitation path shows three lasers ($\lambda_1, \lambda_2, \lambda_3$) passing through a linear polarizer (P_i), apertures (A_1, A_2) and a Fresnel rhomb (FR). The collected light passes through a quarter-wave plate ($\lambda/4$), a linear polarizer (P_d), two lenses (L_1, L_2), an aperture (A_3), and an interference filter.

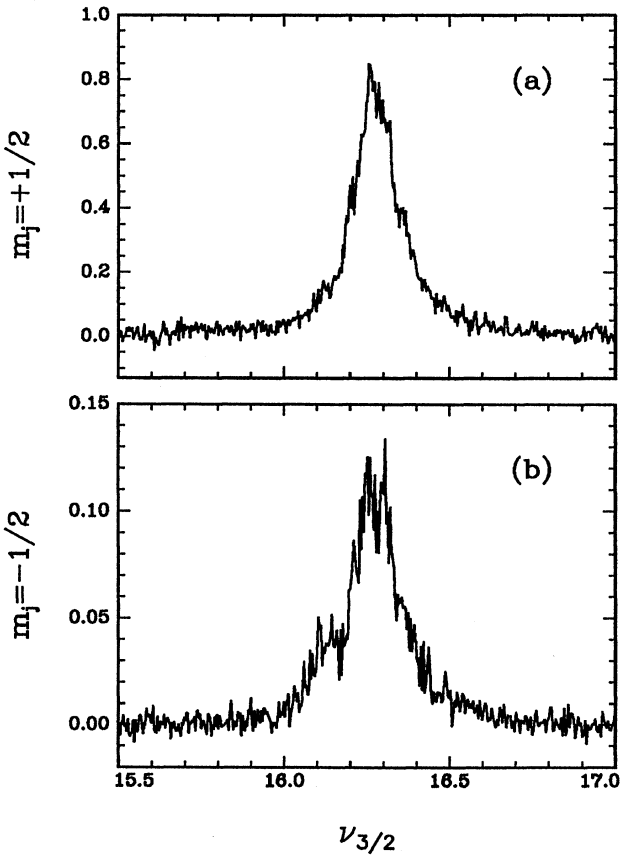

FIG. 3. Typical fluorescence signal after exciting the $(6p_{3/2}19d)_{J=M_J=3}$ state via the $6s19d\ ^1D_2$ intermediate state (which primarily excites + character). The signals show fluorescence from the $6p_{1/2}$ ions in the $m_j = +1/2$ state (a), and $m_j = -1/2$ state (b).

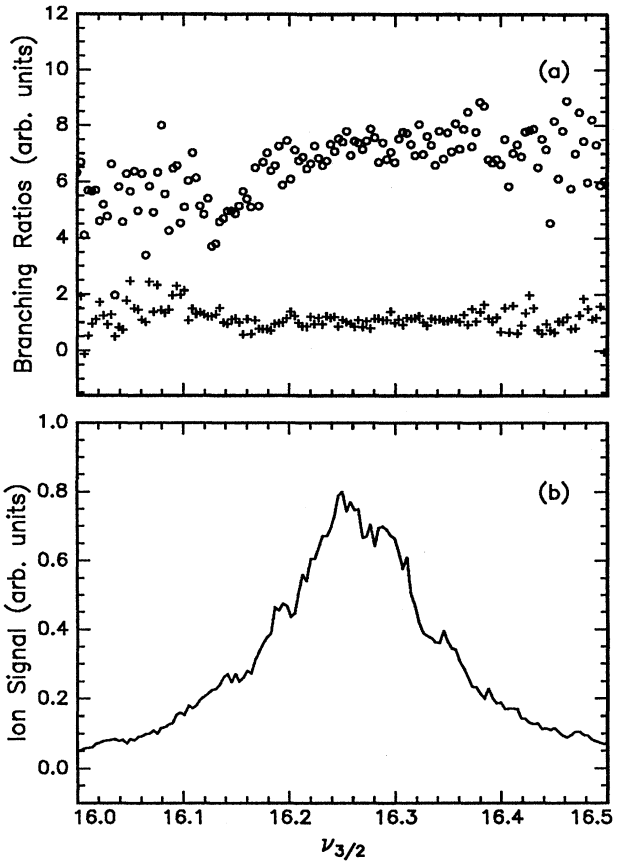

FIG. 4. The relative production of barium $6p_{1/2}$ ions in the $m_j = +1/2$ (○) and $m_j = -1/2$ (+) states following excitation of the $(6p_{3/2}19d)_{J=M_J=3}$ state via the $6s19d\ ^1D_2$ intermediate state (which primarily excites + character). These ratios have been normalized to the value for production of $m_j = -1/2$ ions on resonance. In (b), the total ion production shows that the increased noise at the edge of the spectra is due to the reduced signal size. The horizontal axis shows the effective quantum number relative to the barium $6p_{3/2}$ ionization limit.

ized to the resonant value for the $m_j = -1/2$ state. The branching ratios are nearly constant over a wide energy range, with the branching ratio to the $m_j = +1/2$ state typically being 6–7 times larger than that to the $m_j = -1/2$ state. Using the large signals on the line center, we have measured the ratio of the two fluorescence signals (using the ion signals as calibration), and found that $S_{m_j=+1/2}/S_{m_j=-1/2} = 7.0\pm0.4$. Since the signal in the $6p_{1/2}(m_j = +1/2)$ state results from the sum of all the $6p_{1/2}\epsilon d_{5/2}$ population plus 1/8 of the $6p_{1/2}\epsilon g_{7/2}$ population, while the signal in the $6p_{1/2}(m_j = -1/2)$ state results from the other 7/8 of the $6p_{1/2}\epsilon g_{7/2}$ population, the ratio of the channel populations is $P_d/P_g = 6.0\pm0.4$.

The increased noise at the edges of the spectra is due to the decreased total signal size, as shown by the ion signal of Fig. 4(b). Near the Ba $(6p_{3/2}19d)_{J=3}^-$ resonance (n^*=16.15), the branching ratio to the $m_j = +1/2$ state decreases while the branching ratio for the $m_j = -1/2$ state increases. This change in the branching ratio could be due to the increased excitation of the $(6p_{3/2}19d)^-$ character near its resonance; however, the ion signal shows very little evidence of enhanced excitation. It is more likely that this change represents the effects of the $(6p_{3/2}19d)^-$ resonance on the available continua. Since the + and − resonances have the same symmetry, they will autoionize into linear combinations of the same continua. However, near the energy of the $(6p_{3/2}19d)^-$ resonance, one specific linear combination of continua will be strongly coupled to the $(6p_{3/2}19d)^-$ character and will experience a rapid phase shift. This will change the branching ratio of any state which does not autoionize into orthogonal continua. These data alone are not sufficient for a detailed analysis of these two effects; a multichannel quantum-defect theory calculation, similar to that done for the $J = 1$ states of barium [5] would be very useful for discriminating between these two effects.

Finally, we also recorded ion and fluorescence profiles at high core laser intensities, broadening the profiles and reducing the noise in the wings, but we found no evidence of a modification in the branching ratios near the two $(6p_{3/2}ng)_{J=3}$ states. Although our excitation would not directly excite $6png$ states, these states have the same parity and J value as the $(6p_{3/2}nd)_{J=3}$ states. Just as the unexcited $(6p_{3/2}nd)^-$ state can cause a modification in the branching ratio by its effect on the continua channels, we had expected the unexcited $(6p_{3/2}ng)_{J=3}$ state to also modify the branching ratio. This surprising lack of structure suggests that those $(6p_{3/2}ng)_{J=3}$ states autoionize into a set of continua that is nearly orthogonal to those into which the $(6p_{3/2}nd)_{J=3}$ state autoionizes.

The major sources of systematic error are imperfections in the polarization of the input lasers and in the polarization detection system. We have measured each input laser polarization to be better than 99% pure circularly polarized, and we have determined that the detection system produces no more than 3% polarization scrambling due to off-axis collection. Finally, our quarter-wave plate introduces less than 2% error for a total polarization measurement uncertainty of less than 10%. To verify this, we measured the helicity of the fluorescence from the $6s8d\ ^1D_2$, $M_J = 2$ state (λ=488 nm), which requires two of our three lasers for excitation, and should produce purely circular polarized fluorescence. We detected 7% of the signal with the wrong polarization, consistent with the above analysis, confirming that our polarization error is less than 10%.

A second possible systematic error source is depolarization due to the hyperfine interaction in the 18% of barium with nuclear spin [8]. For example, barium^{137} has $I = 3/2$, which can depolarize the atom during excitation. However, since $\Delta J = \Delta M_J = +1$ are the strongest transition moments, any depolarization during the excitation decreases the subsequent transition moments for that atom. Thus, we estimate that less than 5% of the three-step excited atoms will not be in the $J = M_J = 3$ state. This depolarization would have been somewhat larger for the two-photon excitation of the $6s8d\ ^1D_2$, $M_J = 2$ state (which we used to verify our lasers' polarization), so we are confident that our total systematic error is less than 10%.

Table I lists the results for all of the $(6p_{3/2}nd)^+$ states, from 16 to 23. Each state has a similar ratio of the populations in the $6p_{1/2}\epsilon d_{5/2}$ and $6p_{1/2}\epsilon g_{7/2}$ channels; no significant variations are apparent. These results show that the coupling of the $(6p_{3/2}nd)^+_{J=M_J=3}$ states to the $6p_{1/2}\epsilon g_{7/2}$ continua are smaller than their coupling to the $6p_{1/2}\epsilon d_{5/2}$ waves. The major source of the coupling is likely to be the exchange dipole interaction. Although direct quadrupole coupling is possible for both channels, the angular-momentum coupling factors reduce the effect of the quadrupole coupling strength for F states to be 3.5 times smaller than for P or D states. The $J = 3$ states have a large fraction of F character, and so the quadrupole coupling is therefore reduced.

In conclusion, using an extension of the polarized residual-ion fluorescence detection method, we have measured the ratio of the autoionization products of the Ba $(6p_{3/2}nd)^+_{J=3}$ state into two continua with the same residual ion: Ba $(6p_{1/2}\epsilon d_{5/2})$ and Ba $(6p_{1/2}\epsilon g_{7/2})$. This ratio is nearly constant except for a small region near the $(6p_{3/2}nd)^-_{J=3}$ state, where $6p_{1/2}\epsilon g_{7/2}$ channel production increases and the $6p_{1/2}\epsilon d_{5/2}$ channel production decreases. Over most of the energy range, the $6p_{1/2}\epsilon d_{5/2}$ channel is the dominant decay channel, having 6 times more population than the $6p_{1/2}\epsilon g_{7/2}$ channel.

TABLE I. Fluorescence signal ratios and continuum channel population ratios at the resonance energy for the $(6p_{3/2}nd)^+_{J=M_J=3}$ states with n values from 16–23.

n	$S(m_j = 1/2)/S(m_j = -1/2)$	$\frac{P_g}{P_d + P_g}$
16	7.0±1.0	14%±2%
17	6.8±1.0	15%±2%
18	6.8±1.0	16%±2%
19	7.0±1.0	14%±2%
20	6.1±0.9	16%±2%
21	6.0±0.9	16%±2%
22	5.9±0.9	17%±3%
23	6.7±1.0	15%±2%

This work was supported by the National Science Foundation under Grant No. PHY-9119951.

* Present address: Department of Physics, University of Virginia, Charlottesville, VA 22901.

[1] F. Gounand, T. F. Gallagher, W. Sandner, K. A. Safinya, and R. Kachru, Phys. Rev. A **27**, 1925 (1983).
[2] O. C. Mullins, Y. Zhu, E. Xu, and T. F. Gallagher, Phys. Rev. A **32**, 2234 (1985).
[3] W. E. Cooke, T. F. Gallagher, S. A. Edelstein, and R. M. Hill, Phys. Rev. Lett. **41**, 178 (1978).
[4] R. Kachru, N. H. Tran, P. Pillet, and T. F. Gallagher, Phys. Rev. A **31**, 218 (1985); M. D. Lindsay, L.-T. Cai, G. W. Schinn, C.-J. Dai, and T. F. Gallagher, *ibid.* **45**, 231 (1992).
[5] V. Lange, M. Aymar, U. Eichmann, and W. Sandner, J. Phys. B **24**, 91 (1991).
[6] L. D. Van Woerkom and W. E. Cooke, Phys. Rev. Lett. **57**, 1711 (1986); L. D. Van Woerkom and W. E. Cooke, Phys. Rev. A **37**, 3326 (1988);
[7] G. T. Xu, Xiao Wang, and W. E. Cooke (unpublished).
[8] R. P. Wood, C. H. Greene, and D. Armstrong, Phys. Rev. A **47**, 229 (1993).